Some basic aspects of synchrotron Mössbauer reflectometry

L. Deák, L. Bottyán, M. Major, D.L. Nagy, H. Spiering[a] E. Szilágyi
KFKI Research Institute for Particle and Nuclear Physics, H-1525 Budapest,. POB 49, Hungary, [a]Institut für Anorganische Chemie und Analytische Chemie, Johannes Gutenberg Universität, Staudinger Weg 9, D-55099 Mainz, Germany

Synchrotron Mössbauer reflectometry (grazing incidence nuclear resonant scattering of synchrotron radiation, SMR) is a novel technique capable of depth profiling the hyperfine interactions close to the surface of thin films and multilayers on a nm scale. The principles of SMR are briefly summarised. A picturesque explanation of the appearance of the "total reflection peak" in the time integral delayed photon intensity is presented. It is shown that a fast algorithm for calculating SMR data exists that can be easily deduced both from anisotropic optical model and from the dynamic theory of nuclear resonant x-ray scattering.

1. Introduction

Since its discovery [1], Mössbauer effect has become one of the established tools of studying hyperfine interactions in solids. Interest in hyperfine interactions (HFI) of resonant nuclei embedded in compounds, metals and alloys has been motivated by the sensitivity of the HFI to electronic and, thereby, to atomic and magnetic structure of the environment of the resonant nucleus. In particular, the energy domain Mössbauer spectrum is shifted by an amount of energy (source velocity) proportional to the electron density at the nucleus that is, in turn, closely related to the chemical bond (isomer shift). The electric field gradient which can be deduced from the valence state and from the local symmetry leads to well-defined shift/splitting of the resonance lines (quadrupole shift/splitting). An external or internal magnetic field results in Zeeman splitting of the resonant nuclear transitions. Line intensities are characteristic of crystalline and magnetic texture, line shapes bear information on spatial inhomogeneities and on dynamics of HFI. Knowledge of HFI soon turned out to be extremely useful for identifying certain chemical or intermetallic phases using their Mössbauer spectra as "fingerprints". In addition, Mössbauer spectroscopy proved to be one of the most powerful tools in studying the static and dynamic magnetic structure of compounds, metals and alloys.

During the past few decades, thin films, heterostructures, multilayers, superlattices and interfaces became the most important materials of high technology. Accordingly, there has been an ever increasing demand in methods capable of probing the chemical and magnetic structures of these systems. In other words, depth profiling the HFI became a subject of general interest from the point of view of both basic science and applications. Conventional transmission Mössbauer spectroscopy is not surface sensitive the attenuation depth of 10–80 keV photons typically ranging from a few μm to a few mm. Conversion electron Mössbauer spectroscopy (CEMS) utilises conversion electrons from the resonance process. The attenuation depth of such electrons is typically 100 nm so that in a CEMS experiment about the uppermost 100 nm of a thin film can be investigated. A limited depth selectivity within this range can be achieved by analysing the energy of conversion electrons [2] (depth selective CEMS, DCEMS). Electrons originating from deeper regions lose more energy, while those stemming from layers close to the surface lose less energy. The typical depth resolution of DCEMS is only 20–50 nm. Besides, due to the energy analysis involved, the performance of DCEMS is quite low. The depth resolution of DCEMS may be considerably improved, at the expense of the anyway low counting rate, in the near-surface region. Most depth selective HFI studies on thin films have been performed so far with this method.

Specular reflection of x-rays and neutrons has been widely used to study the structure of thin films, implanted semiconductors and metals, multilayers, superlattices, etc. The corresponding methods, viz. x-ray and neutron reflectometry use the fact that the real part of the index of refraction n of most materials for thermal neutrons and of all materials for x-rays is by about 10^{-5} less then unity. At low enough angles of grazing incidence Θ (for n real, i.e. for negligible absorption $\Theta < \Theta_c = \sqrt{2(1-n)}$) the waves are, therefore, totally reflected from a flat surface. The intensity of the beam of specular reflection for $\Theta > \Theta_c$ rapidly decreases with increasing wave vector transfer $Q = k \cdot \sin\Theta$ where k is the wave vector of the incident radiation. In a stratified medium, reflected and refracted beams appear at each interface. The interference of the reflected beams leads to patterns in $R(Q)$, the reflectivity vs. wave vector transfer curve, that bear information on the depth profile of the index of refraction $n(z)$ the argument z being the co-ordinate perpendicular to the sample surface. (Throughout this paper we shall use the term "reflectivity" in the sense "reflected intensity" while the corresponding amplitude will be called "reflected amplitude". The two quantities will be denoted by R and r, respectively.)

The aim of a reflectometric measurement is to reconstruct $n(z)$ from $R(Q)$ since, as it will be shown below, the depth profile of the index of refraction contains information characteristic of the chemical and magnetic structure of the thin film. Various methods exist for calculation of $R(Q) = |r(Q)|^2$ from $n(z)$ one of them being the *method of characteristic matrices* [3]. The inverse problem, however, viz. reconstructing $n(z)$ from $R(Q)$ can in most cases only be solved in frames of a given model for the stratified system. Additional information like Rutherford backscattering (RBS) experiments, therefore, turns out to considerably enhance the reliability of the evaluation of reflectometric data [4].

The existence of optical models to describe the interaction of x-rays and thermal neutrons on forward scattering and in grazing incidence with condensed matter is based on the fact that the coherent forward scattering of a scalar wave of momentum much higher than that of the scatterers can be described [5] by the index of refraction close to unity

$$n = 1 + \frac{2\pi\, N}{k^2} f \tag{1}$$

where N is the density of scatterers and f is the scattering amplitude. The structural information for condensed matter is implied in the latter quantity. For neutrons, f is the sum of the nuclear and the magnetic scattering lengths b and p, respectively, while for x-rays (far from absorption edges and from nuclear resonances, i.e. Mössbauer transitions) f is determined by the Rayleigh scattering and photoabsorption i.e. by the electron density. Close to a Mössbauer resonance E_0, however, the photon's coherent scattering amplitude f in Eq. (1) is a sum of the electronic and the nuclear coherent scattering amplitudes:

$$f(E) = f^{\mathrm{el}} + f^{\mathrm{nuc}}(E) \tag{2}$$

the latter being a rapidly varying function of the energy around E_0. The nuclear scattering amplitude $f^{\mathrm{nuc}}(E)$ can be expressed in terms of the matrix elements $a_{\alpha\beta}$ of the hyperfine Hamiltonian [6]:

$$f^{\mathrm{nuc}} = \frac{kV}{hc} f_{\mathrm{LM}} \frac{1}{2I_{\mathrm{g}}+1} \sum_{\alpha,\beta} \frac{\left|a_{\alpha\beta}\right|^2}{E-(E_\alpha - E_\beta)+i\frac{\Gamma}{2}} \tag{3}$$

where k is the wave number, V the normalisation volume, f_{LM} the recoilless (Lamb–Mössbauer) fraction, I_{g} the ground state nuclear spin, E_α and E_β are the nuclear excited and ground state energies, respectively (E_α - $E_\beta = E_0$) and Γ is the natural linewidth. For nuclear resonant scattering (NRS), f and n are 2×2 matrices rather than scalars since the two polarisation states of photons should be accounted for [6]. The optical approach based on Eq. (1) is exactly valid for the coherent forward scattering of resonant photons and it is also a good approximation for grazing incident photons in specular reflection [7].

X-ray and neutron reflectometry can be used for mapping the isotopic and the electron density structure of thin films. Besides, neutron reflectometry is an efficient method to study thin film magnetism, as well. A drawback of both methods is, however, their insensitivity for local (hyperfine) interactions.

Close to Θ_c, the penetration depth of the x-rays and γ–radiation is rapidly decreasing with decreasing Θ down to a few nanometers. This fact is the key to grazing incidence Mössbauer spectroscopy (GIMS) a method capable of depth profiling hyperfine interactions. In most GIMS experiments conversion electrons (Total External Reflection Conversion Electron Mössbauer Spectroscopy, TERCEMS) [8,9] are detected. By changing Θ around Θ_c (for the γ–ray energy $E = 14.41$ keV and an α–Fe sample $\Theta_c = 3.8$ mrad) and taking at each angle a CEMS spectrum one can, roughly speaking, adjust the depth at which the thin film is "sampled". The other channel that is often used is that of photons of specular reflection. The approach utilising photons in specular reflection may be called Mössbauer reflectometry (MR) [9–11]. MR is based on the fact that, according to Eqs. (1–3), the refraction index $n(E,z)$, at a certain depth, z, contains information on the hyperfine interactions, i.e. on the chemistry, crystal and magnetic structure of the film. Consequently, by measuring $R(E,\Theta)$ in an MR experiment one can reconstruct the depth profile of chemical compounds containing the resonant nucleus along with their hyperfine electric and magnetic structure. (Since k is practically constant in a Mössbauer experiment, henceforth we shall use Θ rather than Q in the argument of R and r.)

The realisation of MR (like of TERCEMS) is quite time-consuming. Even using a strong Mössbauer source of about 5 GBq activity, the typical time of a measurement at a single Θ value is one week or more. Consequently, data collection time of $R(E,\Theta)$ is several months. The reason for this fact is that the radiation of a radioactive source is unavoidably emitted in the full 4π solid angle a tiny fraction of which (about 5×10^{-6} sterad) really hits the sample. MR should be realised, therefore, utilising a source that generates a well-collimated radiation. This is why synchrotrons are best suited for grazing incidence NRS experiment. This is the approach that we shall call, henceforth, synchrotron Mössbauer reflectometry (SMR). The same method is often referred to as "grazing incidence NRS of SR". We prefer, however, SMR, since it is shorter and emphasises the close relation of this technique to x-ray and neutron reflectometry.

In the present paper we shall outline the basic principles of SRM. Main emphasis will be given to the phenomenon of the “total reflection peak”, i.e. the appearance of a high number of delayed photons close to the critical angle of the electronic total reflection. This quantum phenomenon is the key to all grazing incidence NRS experiments. In the final part of the paper data evaluation aspects of SMR will be discussed. We will show that a fast algorithm for evaluation of SMR data exists that can equally well deduced from both established theories of NRS of photons viz. the Hannon–Trammell and the Afanas’ev–Kagan theories.

2. Synchrotron Mössbauer Reflectometry

Due to its unique characteristics, such as high brilliance, high degree of polarisation, high collimation, small beam size, pulsed time structure, extremely high longitudinal and finite transversal coherence length, tunability, synchrotron radiation (hereafter SR) has rapidly become a powerful tool in solid state physics and materials sciences. Since 1985, the first successful demonstration of NRS [12], the field of hyperfine interactions has also become accessible to SR experiments. In contrast to conventional Mössbauer spectroscopy sensitive to the (energy domain) hyperfine shift and splitting of nuclear transitions NRS of SR shows the effect of hyperfine interactions in form of (time domain) quantum beats.

SMR means measuring the time-dependent reflectivity $R_t(t,\Theta)$, i.e. taking several time-domain grazing incidence spectra after the coherent excitation of the hyperfine split nuclear sublevels by the synchrotron pulse (at $t = 0$) at various angles of grazing incidence Θ and evaluating all these spectra simultaneously in order to determine the depth profile of hyperfine interactions. (Subscript t was introduced only to make a formal difference between the energy and time domain reflectivities.) In other words, the full information is contained in time- and angle-dependent 3D spectra. The theory and some practical aspects of SMR have been recently reviewed [7,13–15].

3. The total reflection peak

In contrast to x-ray and neutron reflectometry, the depth selectivity of MR mainly comes from the Θ-dependence of the penetration depth around Θ_c. In the following we shall show that a high number of delayed photons is always available around Θ_c, a fact of crucial importance for SMR. The presented argumentation is, at certain points, picturesque rather than mathematically exact. A rigorous proof of the mentioned phenomenon was given by Baron et al. [16].

As compared to the nuclear lifetime of the ^{57}Fe Mössbauer level of about 10^{-7} s, the electronic scattering is prompt. In a synchrotron time domain experiment, due to the dead time of the detector and electronics, the delayed photons are detected beginning about 10 ns after the exciting pulse. One would expect that all delayed photons stem from the nuclear scattering and will, therefore, not necessarily have significant contribution around Θ_c.

Since, however, the photon is coherently scattered on the whole system of nuclei and electrons the electronic scattering amplitude also contributes to the reflected amplitude $r(E,\Theta)$ and therefore to the number of delayed photons detected between t_1 and t_2 which is proportional to the integral delayed reflectivity

$$D(\Theta) = \int_{t_1}^{t_2} R_t(t,\Theta)\,dt = \int_{t_1}^{t_2} \left| r_t(t,\Theta) \right|^2 dt \qquad (4)$$

where

$$r_t(t,\Theta) = \frac{1}{\sqrt{2\pi}} \int_{-\infty}^{+\infty} r(E,\Theta) \exp(\frac{-i}{\hbar} Et)\, dE = \mathbf{F}\, r(E,\Theta) \tag{5}$$

and $\mathbf{F}$ denotes the energy-to-time Fourier transformation.

The reflected amplitude of the whole system in the energy domain $r(E, \theta)$ can be re-written as

$$r(E, \theta) = [r(E, \theta) - r^{\mathrm{el}}(\theta)] + r^{\mathrm{el}}(\theta) \tag{6}$$

$r^{\mathrm{el}}(\theta)$ being the amplitude reflected by the electrons (i.e. the reflected amplitude far from resonance) a quantity obviously not depending on E in the μeV energy range of interest (cf. Eq. (2)). Taking the Fourier transform of Eq. (6) we have:

$$\mathbf{F}\, r(E, \theta) = \mathbf{F}\, [r(E,\theta) - r^{\mathrm{el}}(\theta)] + \delta(t) \tag{7}$$

From Eqs. (4), (5) and (7) the integral delayed reflectivity is expressed as

$$\begin{aligned} D(\Theta) &= \int_{t_1}^{t_2} \left|\mathbf{F}\, r(E,\Theta)\right|^2 dt = \int_{t_1}^{t_2} \left|\mathbf{F}\left[r(E,\Theta) - r^{\mathrm{el}}(\Theta)\right] + \delta(t)\right|^2 dt = \\ &\int_{t_1}^{t_2} \left|\mathbf{F}\left[r(E,\Theta) - r^{\mathrm{el}}(\Theta)\right]\right|^2 dt \approx \int_{-\infty}^{+\infty} \left|\mathbf{F}\left[r(E,\Theta) - r^{\mathrm{el}}(\Theta)\right]\right|^2 dt \end{aligned} \tag{8}$$

In Eq. (8) $\delta(t)$ was dropped since $t_1 > 0$ and, after this step, t_1 could be replaced by $-\infty$ since the reflected beam is causal (it cannot appear before the excitation). The Fourier transform preserves the norm:

$$D(\Theta) \approx \int_{-\infty}^{+\infty} \left|\mathbf{F}\left[r(E,\Theta) - r^{\mathrm{el}}(\Theta)\right]\right|^2 dt = \int_{-\infty}^{+\infty} \left|\left[r(E,\Theta) - r^{\mathrm{el}}(\Theta)\right]\right|^2 dE \tag{9}$$

$D(\Theta)$ will be maximum for Θ values for which $|r(E,\Theta) - r^{\mathrm{el}}(\Theta)|$ is high over a large range of E. A satisfactory condition for this is that the reflectivities $R(E,\Theta) = |r(E,\Theta)|^2$ and $R^{\mathrm{el}}(\Theta) = |r^{\mathrm{el}}(\Theta)|^2$ differ significantly from each other over a large range of E. The example shown in Fig. 1 demonstrates that condition is always fulfilled close to the critical angle Θ_c of the total external reflection belonging to the pure electronic scattering, i.e. far from resonance. In fact, in this region the electronic reflectivity is nearly unity while the reflectivity at resonance is strongly damped due to absorption. Therefore, in spite of the fact that the electronic scattering is prompt, it can not be neglected in the time integral delayed reflectivity.

In the previous considerations, when calculating the response to an impulse by the Fourier transformation, we actually used the linearity of the system. The reason for proceeding so was the relatively easy way (the application of the Fresnel law in the simplest case) of calculating the intensities in the energy domain. To give a more picturesque description of the total reflection peak, we have to go back to the time domain. The incoming radiation from a synchrotron source is a delta-like sign, a narrow wave packet propagating with velocity of light. To describe the scattering we take the Fourier components of the incoming wave packet, calculate the reflected amplitude of each spectral component and sum them up. Without having resonant nuclei in the medium all the Fourier components will be multiplied by the non-dispersive factor $r^{\mathrm{el}}(\Theta)$. So after the scattering we shall have the original wave

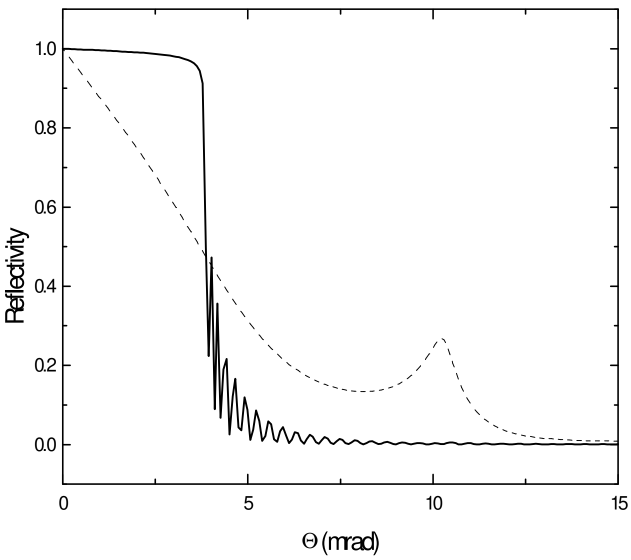

Fig. 1. Calculated reflectivity of a [^{56}Fe(3.0 nm)/ ^{57}Fe(1.5 nm)]$_{20}$ multilayer on glass substrate at resonance (v = 5.3124 mm/s, dashed line) and far from resonance (v = 25.0 mm/s, full line) as a function of the angle of grazing incidence.

packet with a modified amplitude, in other words the electronic (non-dispersive) scattering is prompt. In the presence of resonant nuclei all Fourier components but those very close to the resonant energy E_0 will be multiplied by $r^{el}(\Theta)$. The Fourier components close to E_0, however, will be multiplied by the dispersive reflectivity amplitude $r(E,\Theta)$ significantly differing just in this region from $r^{el}(\Theta)$. The delayed reflectivity appears since the phase of these Fourier components is changed and are no longer able to cancel each other over a long time after excitation. The example in Fig 1. shows that the dispersion is the strongest just at Θ_c and so we expect a peak in the intensity of the delayed photons at this angle.

The existence of the total reflection peak was first predicted by model calculations [17,18]. This peak has also experimentally been observed [16] and, since then, widely used in all synchrotron NRS experiments at grazing incidence. The existence of this peak ensures that a time domain MR, i.e. SMR experiment is always feasible around Θ_c.

4. Anisotropic optics vs. dynamic theory of SMR

The basic problem of SMR data evaluation is to calculate the reflectivity amplitude from the hyperfine parameters and the width of the individual layers. Once this problem has been solved the hyperfine parameters and the layer widths (in a more general case the surface and interface roughnesses, as well) should be varied as long as the best fit to the measured time- and angle-dependent reflectivity $r_t(t,\Theta)$ has not been achieved. It is, therefore, crucial to adopt the fastest possible algorithm to calculate $r_t(t,\Theta)$.

The most widely known general description of NRS was given by Hannon, Trammell et al. [19–22]. Starting from the quantum field theory, they formulated the dynamic theory of Mössbauer optics (henceforth *the dynamic theory*). Beside the general treatment of the forward scattering case [20] (equivalent to that of Blume and Kistner [23]) the grazing incidence optical limit was also studied [20,13] in terms of the forward scattering amplitude. With an extension of the characteristic matrix technique treated in Appendix B of Ref. [21], the grazing incidence optical model [20,21] was implemented in numerical calculations [13].

Afanas'ev and Kagan [24] were the first to formulate a general microscopic theory of NRS. The 3×3 susceptibility tensor χ introduced by them and expressed in terms of the nuclear current density operators was identified, in the optical limit, with the electric susceptibility of the homogeneous nuclear medium. This theory was applied for the grazing incidence limit by Andreeva *et al.* in several papers [10,25–27]. They use the expression of χ given by Afanas'ev and Kagan [24] and a covariant formalism of anisotropic optics by Borzdov *et al.* [28]. Making use of the fact that the elements of the susceptibility tensor χ and also the angle Θ are small, Andreeva *et al.* derived the nuclear reflectivity ("Andreeva approximation" in Ref. [7]). A closed simple form of the reflectivity formulae and a lower limit for Θ in the Andreeva approximation have recently been given by us [7].
The two approaches agree in the forward scattering limit [7,21]. In spite of the general belief, a *formal* equivalence of the relevant theories in the grazing incidence limit has not been shown yet and, consequently, the various numerical implementations unnecessarily differ from each other. Below we show how to map the two approaches in the grazing incidence limit, then numerical considerations are made concerning the efficient evaluation of matrix exponentials involved in the calculation of the reflectivity.
The formula of the dynamic theory [21] describing scattering by a stratified specimen in the grazing incidence limit (Eq. A3 of Ref. [21] in a matrix form) reads

$$\frac{\mathrm{d}}{\mathrm{d}z}\begin{pmatrix} T \\ R \end{pmatrix} = i\begin{pmatrix} g_0 I + G & G \\ -G & -g_0 I - G \end{pmatrix}\begin{pmatrix} T \\ R \end{pmatrix} \tag{10}$$

where z is the co-ordinate perpendicular to the film sample, $g_0 = k\sin\Theta$ is the surface normal component of the wave vector $\mathbf{k}$, Θ is the angle of grazing incidence in the vacuum, and I is the 2×2 unity matrix. $G = \frac{4\pi N}{2k\sin\Theta} f$, N is the density of scattering centres, f is the 2×2 coherent forward scattering amplitude. At a depth z, $T(z)$ and $R(z)$ are the amplitudes of waves incident from above ($z' < z$) and from below ($z' > z$), respectively (for a more rigorous definition of these quantities see Refs. [20,21]). Introducing $\chi = \frac{4\pi N}{k^2} f$ from Eq. (10) we have

$$\frac{\mathrm{d}}{\mathrm{d}z}\begin{pmatrix} T \\ R \end{pmatrix} = ikM\begin{pmatrix} T \\ R \end{pmatrix} \tag{11}$$

with the differential propagation matrix [7,28]

$$M = \begin{pmatrix} I\sin\Theta + \frac{\chi}{2\sin\Theta} & \frac{\chi}{2\sin\Theta} \\ -\frac{\chi}{2\sin\Theta} & -I\sin\Theta - \frac{\chi}{2\sin\Theta} \end{pmatrix}. \tag{12}$$

Eq. (11) now contains the same notations as Ref. [7]. For an arbitrary multilayered film with homogeneous layers of thicknesses d_1, d_2, … d_N and differential propagation matrices M_1, M_2, … M_N, χ is replaced in Eq. (12) by the susceptibility χ_l of layer l. The solution of the differential equation (11) can be expressed in terms of the total characteristic ("integral propagation" [7]) matrix $L = L_N \cdot L_{N-1} \cdot \ldots \cdot L_2 \cdot L_1$ of the multilayer, where

$$L_l = \exp(ikd_l M_l) \tag{13}$$

is the characteristic matrix of the l^{th} individual layer. It is important to note that L_l is the exponential of a 4×4 matrix the numerical calculation of which may be quite time-consuming.

The 2×2 reflectivity amplitude r is obtained from the respective 2×2 submatrices of the 4×4 characteristic matrix L as

$$r = (L_{[22]})^{-1}(L_{[21]})\,. \tag{14}$$

In the special case, when all layers have common eigenpolarisation vectors of χ_l, a simple derivation of the reflectivity is possible, as suggested by Hannon *et al.* [20,21] without using the technique of characteristic matrices.

A somewhat different approach was used by us [7] for the grazing incidence case. Starting with the susceptibility expression χ given by Afanas'ev and Kagan [24] and using the anisotropic optics of Borzdov *et al.* [28] we derived a differential equation similar to Eq. (11), with a differential propagation matrix for layer l of a multilayer

$$M'_l = \begin{pmatrix} 0 & I\sin\Theta + \dfrac{\chi_l}{\sin\Theta} \\ I\sin\Theta & 0 \end{pmatrix} \tag{15}$$

from which the characteristic matrix

$$L'_l = \exp(ikd_l M'_l) \tag{16}$$

and the reflectivity matrix could be calculated in a closed form. For multilayers, the reflectivity matrix [7] is

$$r' = (L'_{[11]} - L'_{[12]} - L'_{[21]} + L'_{[22]})^{-1}(L'_{[11]} + L'_{[12]} - L'_{[21]} - L'_{[22]}) \tag{17}$$

where $L'_{[ij]}$ $(i,j = 1,2)$ are 2×2 blocks of the 4×4 total characteristic matrix $L' = L'_N \cdot L'_{N-1} \cdot \ldots \cdot L'_2 \cdot L'_1$ [7]. Although Eq. (17) seems to be more complicated than Eq. (14), it can be calculated in a more efficient way since, as we shall see, the evaluation of Eq. (2.7) needs only 2×2 matrix exponentials to be calculated for which a simple closed expression exists.

In fact, the characteristic matrix L'_l is of the form [7]:

$$L'_l = \begin{pmatrix} \cosh(F_l) & \dfrac{1}{x_l} F_l \sinh(F_l) \\ x_l F_l^{-1} \sinh(F_l) & \cosh(F_l) \end{pmatrix} \tag{18}$$

where $F_l = kd_l\sqrt{-\sin^2\Theta - \chi_l}$ and $x_l = ikd_l \sin\Theta$.

To evaluate Eq. (18) first we have to calculate the 2×2 square root of the F matrices. This can be made by using the identity [28]

$$G^{1/2} = \frac{G + I\sqrt{\det G}}{\sqrt{\operatorname{Tr} G + 2\sqrt{\det G}}}\,, \tag{19}$$

where G is a 2×2 matrix. The sinh and cosh functions are calculated from their definition with the exp function. The exponential of the 2×2 matrix G can be expressed by G and its scalar invariants [23]:

$$\exp G = \exp\left(\frac{1}{2}\operatorname{Tr} G\right)\left[\cos\sqrt{\det\overline{G}}\,I + \frac{\sin\sqrt{\det\overline{G}}}{\sqrt{\det\overline{G}}}\,\overline{G}\right], \tag{20}$$

where $\overline{G} = G - \frac{1}{2} I \operatorname{Tr} G$.

In order to calculate the characteristic matrix of a semi-infinite substrate layer, we have to find its $d \to \infty$ limes L^{∞}. From Eqs. (15–20) follows that the corresponding limes is given by

$$L^{\infty} = \begin{pmatrix} I & s\sqrt{I + \dfrac{\chi}{\sin^2\Theta}} \\ s\left(\sqrt{I + \dfrac{\chi}{\sin^2\Theta}}\right)^{-1} & I \end{pmatrix} \tag{21}$$

where $s = \operatorname{sgn}[\operatorname{Re}(\operatorname{Tr} F)]$ is the sign of the real part of the trace of F.

A first implementation of the above algebra shows the following characteristics. Using single precision arithmetic in the optical routine the product of up to 16 matrices corresponding to 16 layers could be handled without serious numerical instabilities. Using double precision arithmetic, these figures double. In order to give an idea of effectiveness of the algorithm: on a 166 MHz Pentium processor, a 1024 channel spectrum of 16 resonant layers with one resonant lattice site in each layer needs 0.95 s CPU time, 80 % of which is taken by the optical routine. The corresponding program EFFINO [29] is freely downloadable [30].

Finally we show that the two reflectivity expressions (14) and (17) originating from the Hannon–Trammell [19–22] and the Afanas'ev–Kagan [24] formalism, respectively, are equivalent. In fact, the differential propagation matrices of Eqs. (12) and (15) are related to each other by a unitary transformation:

$$M' = CMC^{-1} \tag{22}$$

with

$$C = \frac{1}{\sqrt{2}}\begin{pmatrix} I & -I \\ I & I \end{pmatrix} \tag{23}$$

From the definition of the matrix exponential follows that the characteristic matrix L is transformed by the same unitary transformation as the differential propagation matrix M, i.e. $L=C^{-1}L'C$ and, expressing L by L' in Eq. (14) finally Eq. (17) (or *vice versa*) is derived.

5. Conclusions

Synchrotron Mössbauer reflectometry is an efficient method of depth selective phase analysis and of studying magnetic structure of thin films and multilayers containing resonant nuclei. Due to the high number of delayed photons appearing close to the critical angle of the electronic total reflection, this method is always of high performance. The depth profile of the hyperfine interactions can be extracted from the angle- and time-dependent reflectivity data utilising an algorithm that is based on calculating matrix exponentials of 2×2 matrices. This algorithm can be easily deduced both from anisotropic optical model and from the dynamic theory of nuclear resonant x-ray scattering.

This work was partly supported by the Hungarian Scientific Research Fund (OTKA) under Contract Nos. F022150 and T029409 and by the Hungarian Academy of Sciences (Contract No. AKP 97–104 2,2/17)

References:

[1] R.L. Mössbauer, *Z. Phys.* **151,** 124 (1958).

[2] Zw. Bonchev, A. Jordanov, A. Minkova, in *Proc. Conf. Appl. Mössbauer Effect, Tihany, 1969*, ed. I. Dézsi, Akadémiai Kiadó, Budapest, 1971, page 333.

[3] M. Born, E. Wolf, *Principles of Optics*, Pergamon Press, Oxford, 1970, page 51.

[4] E. Szilágyi, L. Bottyán, L. Deák, E. Gerdau, V.N. Gittsovich, A. Gróf, E. Kótai, O. Leupold, D.L. Nagy, V.G. Semenov, *Mater. Sci. Forum* **248–249,** 365 (1997).

[5] M. Lax, *Rev. Mod. Phys*. **23,** 287 (1951).

[6] H. Spiering, *Hyp. Int*. **24–26,** 737 (1985).

[7] L. Deák, L. Bottyán, D.L. Nagy, H. Spiering, *Phys. Rev. B.* **53,** 6158 (1996).

[8] J.C. Frost, B.C.C. Cowie, S.N. Chapman, J.F. Marshall, *Appl. Phys. Lett.* **47,** 581 (1985).

[9] S.M. Irkaev, M.A. Andreeva, V.G. Semenov, G.N. Belozerskii, O.V. Grishin, *Nucl. Instrum. Methods B* **74,** 545 (1993).

[10] S.M. Irkaev, M.A. Andreeva, V.G. Semenov, G.N. Belozerskii, O.V. Grishin, *Nucl. Instrum. Methods B* **74,** 554 (1993).

[11] D.L. Nagy, V.V. Pasyuk, *Hyp. Int.* **71,** 1349 (1992).

[12] E. Gerdau, R. Rüffer, H. Winkler, W. Tolksdorf, C.P. Klages, J.P. Hannon, *Phys. Rev. Lett.* **54,** 835 (1985).

[13] R. Röhlsberger in *Nuclear Resonant Scattering of Synchrotron Radiation,* eds. E. Gerdau and H. de Waard, Baltzer Science Publishers, 1999, in press.

[14] D.L. Nagy, L. Bottyán, L. Deák, E. Gerdau, V.N. Gittsovich, J. Korecki, O. Leupold, H. Reuther, V.G. Semenov, E. Szilágyi in *Condensed Matter Studies by Nuclear Methods (Proc. XXXII. Zakopane School of Physics, Zakopane, 10–17 May 1997),* eds. E.A. Görlich and K. Łatka, Institute of Physics, Jagellonian University and H. Niewodniczanski Institute of Nuclear Physics, Kraków, 1997, page 17.

[15] A.I. Chumakov, L. Niesen, D.L. Nagy, E.E. Alp in *Nuclear Resonant Scattering of Synchrotron Radiation,* eds. E. Gerdau and H. de Waard, Baltzer Science Publishers, 1999, in press.

[16] A.Q.R. Baron, J. Arthur, S.L. Ruby, A.I. Chumakov, G.V. Smirnov, G.S. Brown, *Phys. Rev. B* **50,** 10354 (1994)

[17] L. Deák, L. Bottyán, D.L. Nagy in *Condensed Matter Studies by Nuclear Methods (Proc. XXVIII. Zakopane School of Physics, Zakopane, 9–15 May 1993),* eds. E.A. Görlich and K. Tomala, Institute of Physics, Jagellonian University and H. Niewodniczanski Institute of Nuclear Physics, Kraków, 1993, page 269.
[18] L. Deák, L. Bottyán, D.L. Nagy, *Hyp. Int.* **92,** 1083 (1994).
[19] J.P. Hannon, G.T. Trammell, Phys. Rev. **169,** 315 (1968).
[20] J.P. Hannon, G.T. Trammell, Phys. Rev. **186,** 306 (1969).
[21] J.P. Hannon, N.V. Hung, G.T. Trammell, E. Gerdau, M. Mueller, R. Rüffer, H. Winkler Phys. Rev. B **32,** 5068 (1984).
[22] J.P. Hannon, G.T. Trammell, M. Mueller, E. Gerdau, R. Rüffer, H. Winkler, Phys. Rev. B **32,** 6363 (1985).
[23] M. Blume, O.C. Kistner, Phys. Rev. **171,** 417 (1968).
[24] A.M. Afanas'ev, Yu. Kagan, Sov. Phys.–JETP **21,** 215 (1965).
[25] M.A. Andreeva, S.M. Irkaev, V.G. Semenov, Sov. Phys.–JETP **78,** 965 (1994).
[26] M.A. Andreeva, R.N. Kuz'min in *Messbauerovskaya Gamma-Optika*, Moscow University, 1982.
[27] M.A. Andreeva, K. Rosete, Poverkhnost' **9,** 145 (1986); Vestnik Mosk. Univ. Ser. 3. Fiz. Astron. **27,** 57 (1986).
[28] G.M. Borzdov, L.M. Barskovskii, V.I. Lavrukovich, Zh. Prikl. Spektrosk. **25,** 526 (1976).
[29] H. Spiering, L. Deák, L. Bottyán in *Nuclear Resonant Scattering of Synchrotron Radiation,* eds. E. Gerdau and H. de Waard, Baltzer Science Publishers, 1999, in press.
[30] H. Spiering, *EFFI — concept of a fit environment*, donwloadable from http://www.kfki.hu/~mixhp/doc/proidx.htm